

Azide Thermolysis Frameworks: Self-inflating, Porous, and Lightweight Materials

Julian Brückel,^[a, b] Yannick Matt,^[a] Lisa Schmidt,^[b] Cornelia M. Mattern,^[a] Ute Schepers,^[d] Sonja Leopold,^[d] Martin Calkovsky,^[e] Dagmar Gerthsen,^[e] and Stefan Bräse*^[a, b, c]

Abstract: Porous organic materials have received increasing attention due to their potential applications, such as gas storage, gas separation, and catalysis. In this work, we present a series of aromatic, polyazide-containing building blocks that enable the formation of a new class of amorphous porous organic materials. The azide precursors are obtained in moderate to good yields following an easy synthesis procedure. By thermal decomposition, self-inflating porous structures named Azide Thermolysis Frameworks (ATFs) can be obtained. Modified thermogravimetric analysis is used to determine the onset temperature at which the azides

decompose and the frameworks are formed. The frameworks are further investigated *via* infrared (IR) spectroscopy, elemental analysis, scanning electron microscopy (SEM), and gas adsorption measurements. Specific surface areas and pore sizes are determined by nitrogen adsorption measurements at 77 K using the Brunauer–Emmett–Teller method (BET) to give surface areas of up to 677 m²/g for the ATF resulting from the thermolysis of TPB-Azide at 450 °C, which can compete with early Covalent Organic Frameworks (COFs). The specific surface area can be tuned by varying the thermolysis temperature.

1. Introduction

The interest in porous materials increased rapidly in the last two decades due to their potential application in gas storage, gas separation, CO₂ capture, and many others.^[1] For these applications, numerous porous materials have been developed. Besides inorganic porous materials like zeolites and inorganic-organic hybrid materials (e.g., MOFs), organic porous materials are of great interest in current research due to their high

surface areas, tunable structures, well-defined structures porosities, and low densities.^[2]

Porous organic materials can be divided into crystalline materials, including Covalent Organic Frameworks (COFs) and Porous Organic Cages (POCs), as well as amorphous structures like Porous Aromatic Frameworks (PAFs) and Hyper Crosslinked Polymers (HCPs).^[1c] Since the formation of amorphous porous polymers does not require reversible reactions, the building blocks can be connected by a wide range of reactions, e.g., by YAMAMOTO and SONOGASHIRA-HAGIHARA (cross-)coupling^[3] or by FRIEDEL-CRAFT alkylation.^[4] Furthermore, the formation of porous structures by copper-catalyzed azide-alkyne cycloadditions (CuAAC) has been reported.^[5]

In this work, we used the extraordinary chemistry of azides and nitrenes, formed by the thermolysis of azides, to build amorphous, porous frameworks called Azide Thermolysis Frameworks (ATFs). The chemistry of azides has been extensively studied in the past; nevertheless, frameworks resulting from the decomposition of azides *via* the formation of nitrenes have not been reported yet. This new class of frameworks, with specific surface areas compared to the first COFs,^[6] offer the benefit of producing only nitrogen without the need for catalysts or solvents. Besides synthesizing the building blocks and the frameworks, we analyzed them by IR, elemental analysis, and SEM, and the specific surface areas determined according to the BET theory.

In this context, we would like to mention that organic azides are potentially explosive compounds. Further information on the safe handling of azides can be found in the supporting information.

[a] J. Brückel, Dr. Y. Matt, C. M. Mattern, Prof. S. Bräse
Institute of Organic Chemistry (IOC)
Karlsruhe Institute of Technology (KIT)
Fritz-Haber-Weg 6, 76131 Karlsruhe (German)
E-mail: braese@kit.edu

[b] J. Brückel, L. Schmidt, Prof. S. Bräse
3DMM2O-Cluster of Excellence (EXC-2082/1-390761711)
KIT
Fritz-Haber-Weg 6, 76131 Karlsruhe (Germany)

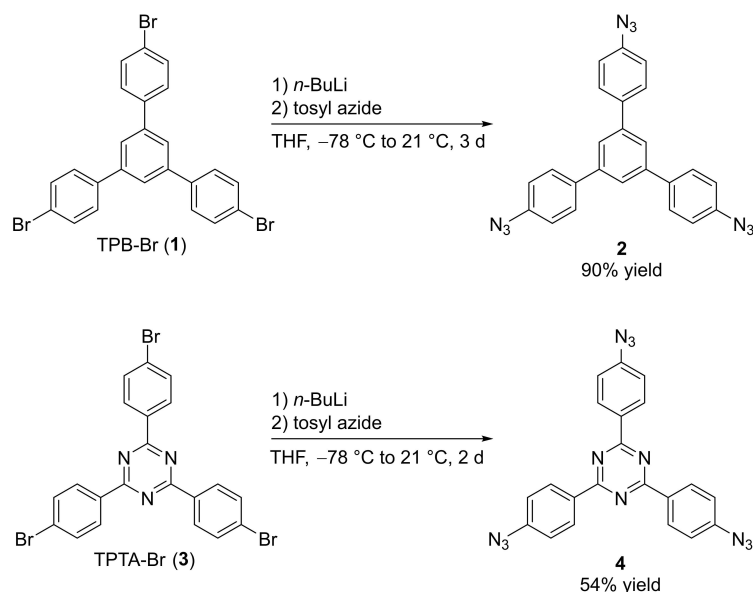
[c] Prof. S. Bräse
Institute of Biological and Chemical Systems-Functional Molecular Systems (IBCS-FMS)
KIT
Hermann-von-Helmholtz-Platz 1, 76344 Eggenstein-Leopoldshafen (Germany)

[d] U. Schepers, S. Leopold
Institute of Functional Interfaces
KIT
Hermann-von-Helmholtz-Platz 1, 76344 Eggenstein-Leopoldshafen (Germany)

[e] M. Calkovsky, Prof. D. Gerthsen
Laboratory for Electron Microscopy
Karlsruhe Institute of Technology (KIT)
Engesserstr. 7, 76131 Karlsruhe (Germany)

 Supporting information for this article is available on the WWW under <https://doi.org/10.1002/cnma.202300222>

 © 2023 The Authors. ChemNanoMat published by Wiley-VCH GmbH. This is an open access article under the terms of the Creative Commons Attribution License, which permits use, distribution and reproduction in any medium, provided the original work is properly cited.



Scheme 1. Synthesis of aromatic azides **2** and **4** using the respective brominated core (**1** and **3**), *n*-BuLi, and tosyl azide.

2. Results and Discussion

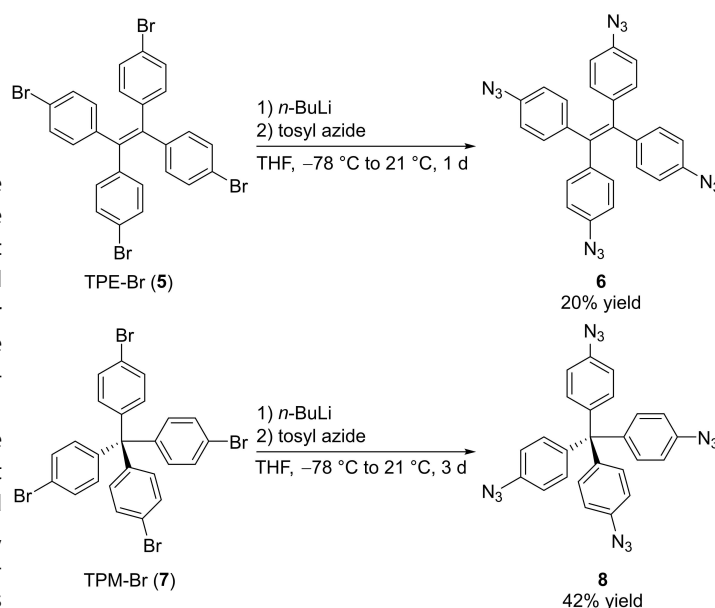
2.1. Synthesis of Polyazides

Aryl azides are readily accessible either by diazotization of the respective aromatic amine and subsequent replacement of the diazonium salt or *via* lithiation of the corresponding aromatic bromide and a suitable azide transfer reagent such as tosyl azide (see supporting information for synthesis). The latter method was chosen to synthesize the polyazides since the brominated precursors can be obtained in a one-step multi-gram scale with high yields.

An optimized procedure was used for the synthesis of the polyazides. It must be noted that the reaction takes place at each bromine atom, and even a low overall yield indicates good to excellent yields for each respective bromine atom. Therefore, the brominated precursor was reacted with *n*-butyllithium (*n*-BuLi) in dry THF at -78 °C, and the azide transfer reagent was added; the reaction times ranged from 1 to 6 days, depending on the precursor. Azide **2** was synthesized from 2,4,6-tris(4-bromophenyl)-benzene (TPB) (**1**) in an overall yield of 90% after recrystallization from ethyl acetate. Lithiation of 2,4,6-tris(4-bromophenyl)-1,3,5-triazine (TPTA) (**3**) and treatment with tosyl azide gave the corresponding azide **4** in a yield of 54% (Scheme 1).

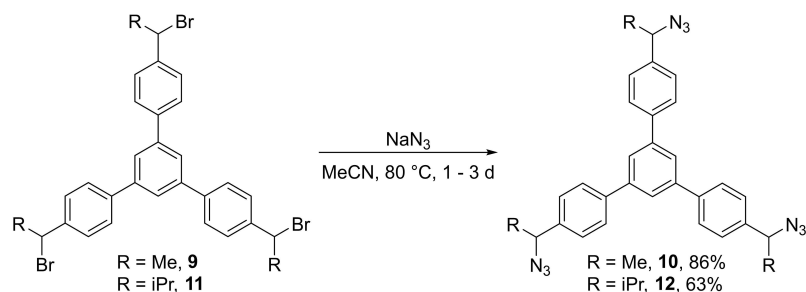
Transferring those conditions, tetrakis(4-bromophenyl)ethylene (TPE) (**5**) and tetrakis(4-bromophenyl)methane (TPM) (**7**) gave the respective polyazides **6** and **8** in yields of 20% and 42% (Scheme 2). In addition, the hexaazide containing the hexaphenyl-*p*-xylene (HPX) core and tetraazidophthalocyanine were synthesized (see supporting information for synthesis).

ATFs are mainly formed by the thermolysis of aromatic azides. To investigate whether aliphatic azides can also form



Scheme 2. Synthesis of aromatic azides **6** and **8** using the respective brominated core (**5** and **7**), *n*-BuLi, and tosyl azide.

ATFs, **10** and **12** were synthesized *via* nucleophilic substitution of the corresponding aliphatic bromines **9** and **11** with sodium azide in acetonitrile; both were isolated in yields of 86% and 63% (Scheme 3).



Scheme 3. Synthesis of the aliphatic azides **10** and **12** using the respective aliphatic bromide (**9** and **11**) and sodium azide.

2.2. Synthesis and Characteristics of ATFs

2.2.1. Synthesis of ATFs and thermogravimetric analysis

The synthesized aromatic azides were converted into ATFs by thermolysis of the respective azide at different temperatures under an ambient atmosphere. Due to their chemical structure, the formation of ATFs is comparable to a small explosion; after heating, the compounds nitrogen is released, resulting in a highly inflated framework. Therefore, the azides were placed in an Erlenmeyer flask and covered to dissipate the nitrogen without losing the ATF. In the case of **2** and **4**, perforated aluminum foil was sufficient to prevent the loss of the ATF during framework formation. For **6** and **8**, the framework formation was more violent. In this case, a watch glass replaced the aluminum foil. Azides **10** and **12** were thermolyzed according to the same procedure to investigate whether aliphatic azides can also form organic frameworks. The thermolysis experiments revealed that instead of framework

formation, the aliphatic azides decomposed completely. Based on these results, it can be assumed that aromatic azides are required to generate ATFs. Gravimetric analysis after thermalization was performed to determine at which temperature framework formation occurs. The oven in which the analysis was carried out was preheated to a predefined temperature between 200 °C and 600 °C, then approximately 10 mg of the azide was added and thermolyzed for 30 min. The corresponding onset temperature of the ATF formation was determined visually; the temperature was set when the azide did not only decompose but generated frameworks.

Furthermore, the weight of the generated ATFs was compared with the weighed amount of the respective azide. This method allowed us to determine the weight loss at a given temperature. Two distinct regions can be seen after plotting the results for each azide (Figure 1B). The first region starts at around 250 °C and extends slightly above 400 °C. None of the azides showed any significant mass loss in this plateau region. The plateau region is slightly shifted towards lower temper-

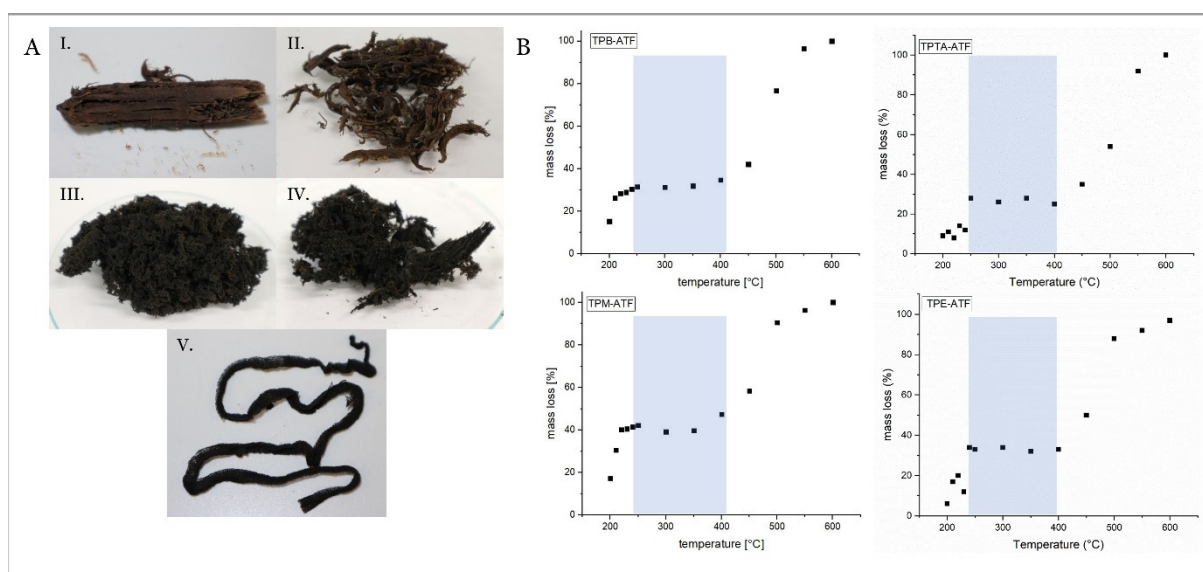


Figure 1. A) Macroscopic ATF-appearance thermolyzed at 250 °C: I. TPB-ATF; II. TPTA-ATF; III. TPM-ATF; IV. TPE-ATF (obtained from fine powder); V. TPE-ATF (obtained from thin flakes). B) Graphs of the thermogravimetric analysis, the mass loss is plotted as a function of the temperature. The prominent plateau region is marked in blue.

atures depending on the azide. After the first plateau region at 400 °C, a different behavior for the ATFs is visible. For TPB-ATF, a steep increase in mass loss is observed after 400 °C, reaching its maximum at around 600 °C. At this temperature, no residue of the azide was detected. The same behavior was observed for TPM-ATF and TPE-ATF, with the only difference being that the plateau region is end shifted towards lower temperatures. TPTA core structure showed the same plateau region as TPM- and TPB-ATF, but instead of a complete mass loss, a second plateau region between 500 °C and 600 °C can be observed; a fine-fibered residue was formed at this temperature. It was found that the temperature of the ATF generation was between 200 °C and 250 °C in the case of the TPB-ATF, TPTA-ATF, TPM-ATF, and TPE-ATF.

2.2.2. Macroscopic Properties of ATFs

The investigated ATFs were generated at approximately 250 °C, where the onset temperature was determined. All azides expanded strongly during thermolysis, showing a unique appearance on a macroscopic scale. The strong inflation of the frameworks mainly occurred due to the loss of nitrogen compared to the inflating polyurethane foams caused by CO₂. Haptic-wise, the frameworks differ depending on the used core structure. For the TPB-ATF and the TPTA-ATF, the obtained frameworks are brittle, whereas the TPM-ATF and TPE-ATF are softer and not fragile. The generated ATFs can be distinguished due to their macroscopic appearance based on their respective geometry of the core structure. Based on the geometry of the core structures, the ATFs can be distinguished since their presence differ significantly in a reproducible manner. Trigonal-planar core structures with three azide functionalities (TPB and TPTA) gave brown ATFs preferentially growing in one specific direction. The appearance of the ATF obtained from TPB-ATF can be described as charcoal-like, while TPTA-ATF gave snake-like pieces. The macroscopic appearance of the ATFs is shown in Figure 1A.

TPM-ATF containing a tetrahedral core gave a framework with a cotton-like structure, showing an expansion in all directions. In contrast, the square planar TPE core gave ATFs similar to the black cotton-like structure obtained by TPM-ATF. Additionally, the thermolysis of TPE-ATF gave frameworks with a ribbon-like appearance. Notably, the ATFs from the TPE core were obtained from different batches; the cotton-like ATF was generated from a fine powder, whereas the ATF-forming ribbons were obtained from thin flakes. This observation indicates that at least for the TPE core, the shape of the framework can be controlled by the crystallinity of the starting material.

Additionally, the hexaazide containing the HPX core was thermolyzed. In contrast to the TPB, TPM, TPB, and TPE core, no self-inflating framework was obtained, and therefore, no further investigations have been performed.

All frameworks generated by thermolysis were insoluble in a broad range of common organic solvents, e.g., dichloromethane, chloroform, ethyl acetate, tetrahydrofuran, methanol,

diethyl ether, dimethyl sulfoxide, *N,N*-dimethylformamide. This indicates that the ATFs are highly crosslinked organic polymers.

2.2.3. Compositional Analysis via IR and elemental analysis

Due to the wide range of reactions that could occur during azide thermolysis, analyzing the resulting ATFs is very challenging. To get insights into bonding types responsible for the connection of the respective building block and, thus, the nature of the framework formation, the ATFs generated by thermolysis were investigated using IR spectroscopy and elemental analysis. ATFs generated at 250 °C were investigated to avoid the detection of undesired side reactions, which can occur at higher temperatures.

The IR spectrum of the ATFs clearly shows the absence of the asymmetric stretching band of the azide functionality at around 2100 cm⁻¹, indicating a complete conversion of all azides into nitrenes at a temperature of 250 °C (Figure 2B). In the starting material, the prominent azide bond at 2100 cm⁻¹ can be observed (Figure 2A). Nitrenes generated by the thermolysis of azides can form nitriles, ketenimines, and azo bonds or insert into a C–H bond to form secondary amines (for a detailed description, see Scheme S1). These reactions could lead to a connection between the building blocks, which resemble either triazine (nitrile trimerization), ether-bridged azepines (reaction of ketenimines with water), azobenzene (formation of azo bonds), or a substituted diphenylamine (insertion into C–H).^[7] Subsequently, the IR spectra of the ATFs were compared to those of diphenylamine and azobenzene. No strong indication for the presence of triazine moieties or ether functionalities and no similarity to the spectrum of azobenzene could be found.^[8] However, strong similarities between diphenylamine and the ATFs were observed. The ATF spectra gave the same peak between 3409 cm⁻¹ and 3384 cm⁻¹, referring to the N–H stretching, which was also observed in the spectra of diphenylamine. Additionally, a peak at 3050 cm⁻¹ in the ATF spectra can be assigned to the aromatic C–H stretching vibration, which is also described for diphenylamine at 3043 cm⁻¹.^[9] The observed peak at 2220 cm⁻¹ is not present in the IR spectrum of diphenylamine; based on the elements contained and the wavenumber, it could be assigned to the stretching vibration of a C≡C, a C≡N or a C=C=N bond of a ketenimine structure or a nitrile, suggesting that formed nitrenes can also react intramolecularly. In all ATFs, a peak at 1600 cm⁻¹ and 1590 cm⁻¹ is visible, corresponding to the stretching vibration of a C=C bond of an aromatic ring. The peak at 1500 cm⁻¹ and 1360 cm⁻¹ seen in the spectrum of TPTA-ATF (Figure 2B) originates from the triazine backbone and can also be observed in the starting material azide **4** (see supporting information). To determine the substitution pattern of the building blocks, the out-of-plane C–H bending vibrations in the region of 900 cm⁻¹–700 cm⁻¹ were investigated. A strong peak at about 800 cm⁻¹ is seen in the generated ATF and the starting material, indicating that the phenyl rings are para-substituted. Furthermore, small peaks around 900 cm⁻¹, 750 cm⁻¹, and 700 cm⁻¹ suggest a different substitution pattern

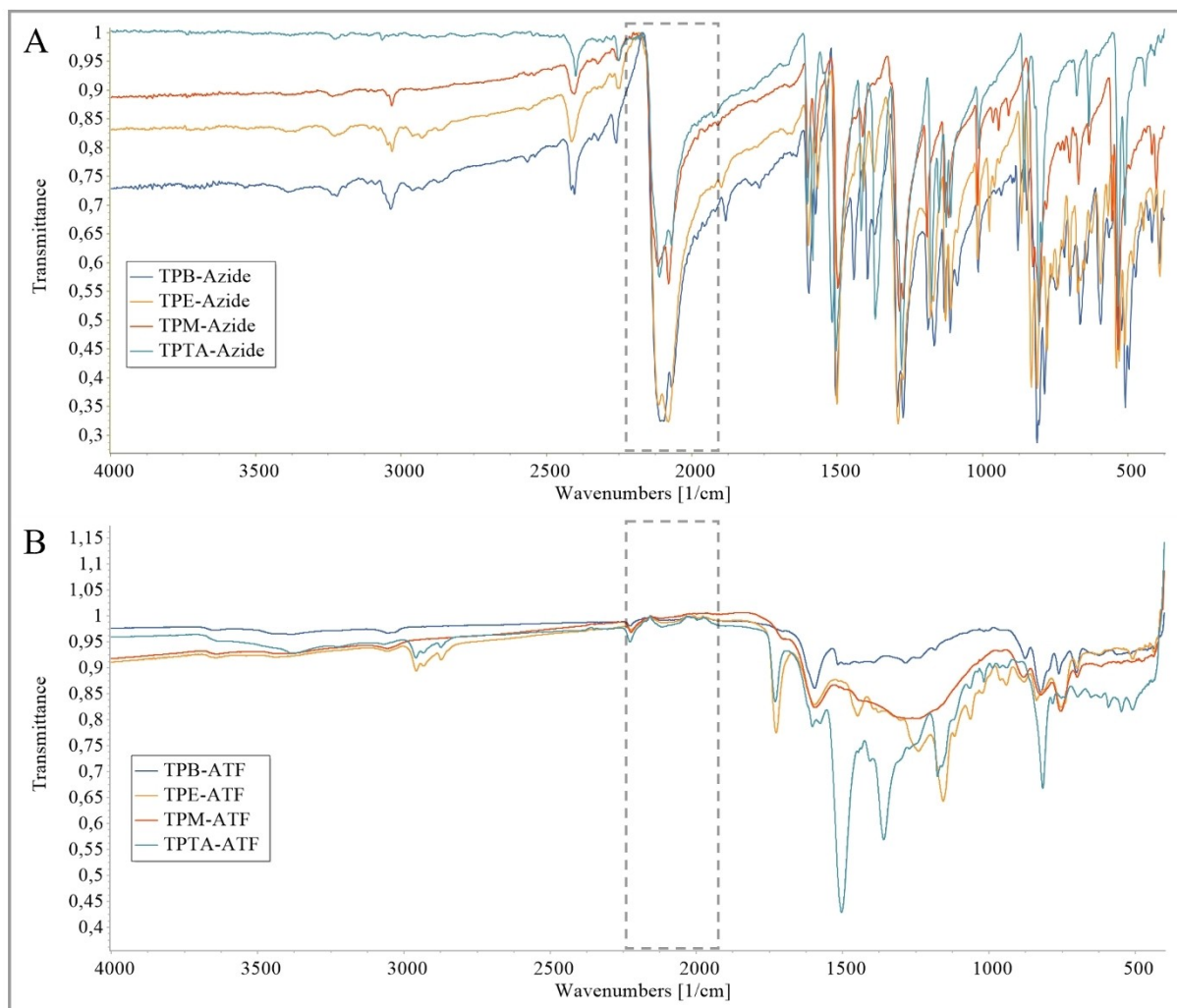


Figure 2. Comparison of the normalized IR-spectra of the building blocks and ATFs thermolyzed at 250 °C. A) IR spectra of the respective aromatic building block with the prominent azide band at 2100 cm⁻¹. B) IR spectra of the generated ATFs. The significant azide stretching band is missing, indicating the complete azide decomposition during thermolysis.

alongside the para-pattern, as it would be assumed when the formed nitrene inserts into a nearby aromatic C–H bond.

Elemental analysis was carried out to investigate the elementary composition of the generated ATFs. For all ATFs, the elemental analysis gave higher carbon, respectively lower hydrogen values. However, all generated ATFs have a drastic loss of nitrogen in common, resulting in a significantly lower nitrogen value than calculated for the idealized nitrenes (see Table 1).

The results from the elemental analysis were used to obtain an empirical sum formula for the generated ATFs to get a more precise evaluation, whereby it was assumed that the difference to 100% was oxygen. Since the thermolysis of the azides was carried out at the lowest possible temperature, it was presumed that the carbon framework of the core structures remained intact. The obtained nitrene formula was compared with the empirical sum formula of the ATFs.

Table 1. Elemental analysis of ATFs thermolyzed at 250 °C and calculated for the respective nitrenes.

Framework	Nitrene (calc.) ^[a]	ATF (found)
TPB-ATF	C 83.46% H 4.38% N 12.17%	C 85.15% H 3.43% N 7.86%
TPTA-ATF	C 72.40% H 3.47% N 24.12%	C 77.20% H 3.69% N 19.7%
TPM-ATF	C 80.63% H 4.22% N 15.04%	C 86.63% H 2.24% N 9.12%
TPE-ATF	C 81.23% H 4.19% N 14.57%	C 83.52% H 2.24% N 5.78%
Pc-ATF	C 61.02% H 1.92% N 26.68%	C 51.87% H 2.89% N 21.6%

^[a] Calculations were performed using the Elemental Composition Calculator of the University of Illinois.

Table 2. Comparison of the idealized sum formulas of the nitrenes and the sum formulas of the ATFs thermolyzed at 250 °C. The sum formulas of the ATFs were calculated from the elemental analysis results.

Framework	Formula Nitrene	Formula ATF
TPB-ATF	C ₂₄ H ₁₅ N ₃	C ₂₄ H _{11.6} N _{1.91} O _{0.75}
TPTA-ATF	C ₂₁ H ₁₂ N ₆	C ₂₁ H _{11.9} N _{4.59}
TPM-ATF	C ₂₅ H ₁₆ N ₄	C ₂₅ H _{8.45} N _{2.077}
TPE-ATF	C ₂₆ H ₁₆ H ₄	C ₂₆ H _{8.30} N _{1.50} O _{1.98}
Pc-ATF-250	C ₃₂ H ₁₂ N ₁₂ Zn	C ₃₂ H ₂₁ N _{11.4} ZnO _{6.95}

Compared to the empirical formula of the respective nitrene, a loss of hydrogen and nitrogen was observed for the TPB-ATF, TPTA-ATF, TPM-ATF, and TPE-ATF. The loss rose from the TPB core, which lost one-third of all its nitrogen, to the TPE core, which lost more than half of its nitrogen, while the amount of oxygen increased (see Table 2). The ATF generated from the TPTA core differs in this respect, as it does not contain oxygen. In the case of the Pc-ATF, the hydrogen content was far above the target value, and a high amount of oxygen was in the sample. Therefore, it was assumed that water was adsorbed on the surface of this ATF.

Due to the insolubility of the frameworks, solid-state NMR was measured from TPB-azide and TPB-ATF, thermolyzed at 250 °C, to further analyze the framework. The broad signals in the ATF ¹³C NMR confirm that the framework has an amorphous structure. Compared to the azide spectrum, the peak at 121 ppm in the ATF spectrum is shifted to higher ppm, indicating a changed chemical environment (Figure 3). However, this does not explain further the reactions that took place during pyrolysis.

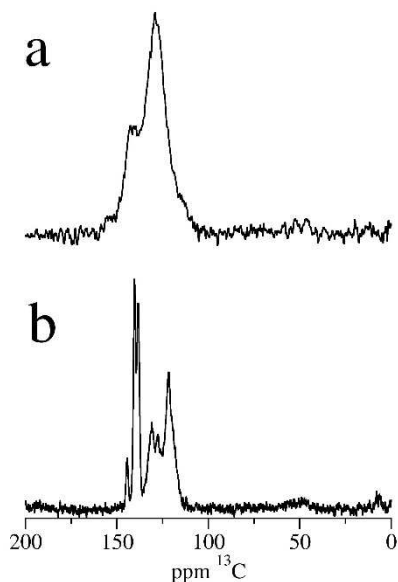


Figure 3. ¹³C NMR solid state of (a) TPB-ATF-250 and (b) TPB-azide

2.2.4. Surface Area, Pore Size, and Density

The specific surface area (SSA) represents a very important property of organic frameworks. To investigate the SSA of the respective ATFs, adsorption isotherms at 77 K were measured for the azides thermolyzed at 250 °C, 350 °C, and 450 °C. The pore size distributions and pore volumes are given in the supporting information.

An initial SSA of 422 m²/g at 250 °C was measured for ATF-TPB. Thermolysis at 350 °C gave an ATF with a slightly increased SSA of 495 m²/g. After thermolysis at 450 °C, an ATF with an immensely increased surface area of 677 m²/g was generated. Determination of the pore size distribution gave pore diameters for all temperatures in the micropore region ranging from 1 nm to 1.50 nm with some mesopores.

The TPTA core gave an ATF with SSAs of 67 m²/g at 250 °C, 161 m²/g at 350 °C, and 234 m²/g at 450 °C, respectively. Interestingly, the pore diameters decreased from initially 1.75 nm to diameters ranging from 0.98 nm to 1.50 nm, only in the framework generated at 450 °C mesopores were observed.

Thermolysis of the TPM core gave an ATF with a relatively low SSA with values below 45 m²/g at 250 °C and 97 m²/g at 350 °C, respectively. Notably, a drastic increase in the SSA to 500 m²/g at 450 °C was measured. At 250 °C, no micropores were observed, whereas thermolysis at 350 °C and 450 °C gave ATFs possessing micropores with diameters in the range of 1.50 nm for the ATF generated at 350 °C and 0.98 nm to 1.50 nm for the ATF generated at 450 °C. Like the TPTA-ATF, mesopores were found at 450 °C.

TPE-ATF generated at 250 °C gave an SSA of 119 m²/g, which increased to 378 m²/g at 350 °C, and finally gave an SSA of 404 m²/g for the ATF generated at 450 °C. Determination of the pore size revealed micropores with diameters between 1.10 nm and 1.50 nm. Mesopores were only found in the ATF generated at 450 °C. In the case of the Pc-ATFs, no significant SSA could be obtained. Nevertheless, it could be proven via EDX spectroscopy that the zinc atoms are still present in the Pc-ATF (Figure S3), making it interesting for application, e.g., in catalysis or conductivity.

All ATFs show a significant increase in the SSA at higher temperatures; for TPM-ATF, even a drastic increase of the surface was observed at 450 °C. Furthermore, a higher temperature, in some cases, shifted the generated pores to lower diameters. Despite the initial SSA, only a minor change in the SSA of the ATFs was observed in the plateau region between 250 °C and 350 °C. Thermalization at 450 °C gave ATFs with an extremely increased SSA; most notable is the increase of the

SSA from the framework generated from the TPM core structure (see Table 3).

In general, thermolysis at a temperature of 450 °C resulted in ATFs with the largest SSA. This observation can be explained by the thermal decomposition of the ATFs at higher temperatures, which could open previously blocked pores. Comparing TPB-ATF and TPTA-ATF generated from trigonal planar core structures reveals another interesting aspect. Even though both ATFs were obtained from trigonal planar azides, a major difference in the SSA was measured. Both building blocks interact strongly with each other *via* aromatic π - π interactions. Due to the strongly polarized bonds, the π - π interactions between the TPTA building blocks are significantly stronger than the TPB building block and thus prevent the strong expansion during thermolysis. In summary, TPM-ATF and TPB-ATF gave frameworks with the highest specific surface area of 677 m²/g and 506 m²/g, respectively. Compared with early Covalent Organic Frameworks like COF-1 with an SSA of 711 m²/g or older Porous Organic Frameworks, the generated

ATFs can compete with those, especially when considering the simple synthesis of the ATFs and their precursors.^[10]

The density of three ATF determined by helium gas pycnometry with 1.97 ± 0.12 for TPB-ATF-350, 2.00 ± 0.06 for TPM-ATF-350, and 1.82 ± 0.07 for TPTA-AATF-350.

2.2.5. Scanning Electron Microscopy

To get greater insights into the surface topography of the ATFs, scanning electron microscopy (SEM) was carried out. All ATFs investigated by SEM were thermolyzed at 250 °C and coated with 12 nm platinum since they are non-conductive materials. Figure 4 shows SEM images taken at different magnifications to investigate structural features between 10 nm to several 100 nm.

The general structure of TPB-ATF shows growth in a preferred direction, which can also be observed macroscopically. Frameworks generated from the TPB core usually exhibit a

Temperature	TPB-ATF	TPTA-ATF	TPM-ATF	TPE-ATF	Pc-ATF
250 °C	422 m ² /g	67 m ² /g	45 m ² /g	119 m ² /g	23 m ² /g
350 °C	495 m ² /g	161 m ² /g	97 m ² /g	378 m ² /g	21 m ² /g
450 °C	677 m ² /g	234 m ² /g	506 m ² /g	404 m ² /g	23 m ² /g

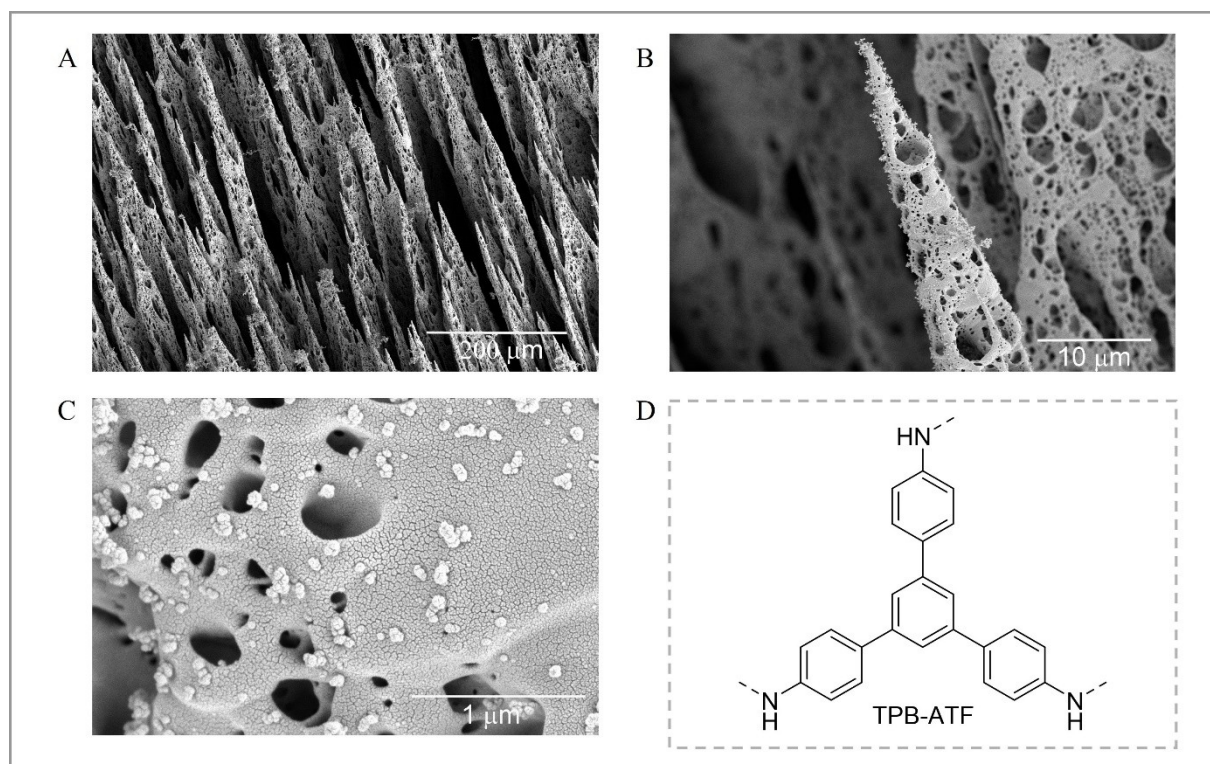


Figure 4. SEM images of TPB-ATF thermolyzed at 250 °C taken at an electron energy of 2 keV in the secondary electron mode. A) Low-magnification overview image of the TPB-ATF columns with cone-like structures with dimensions between several 10 nm up to about 100 nm. B) Cone-like structure of the TPB-ATF with pores ranging from 100 nm to several micrometers. C) High-magnification SEM image of the surface of a TPB-ATF cone with pores in size range from 10 nm to several 100 nm and cracks with widths of about 10 nm. The sputtered Pt-surface layer with 12 nm thickness prevents detecting small pores with sizes in the few-nanometer range. D) Molecular unit of the TPB-ATF.

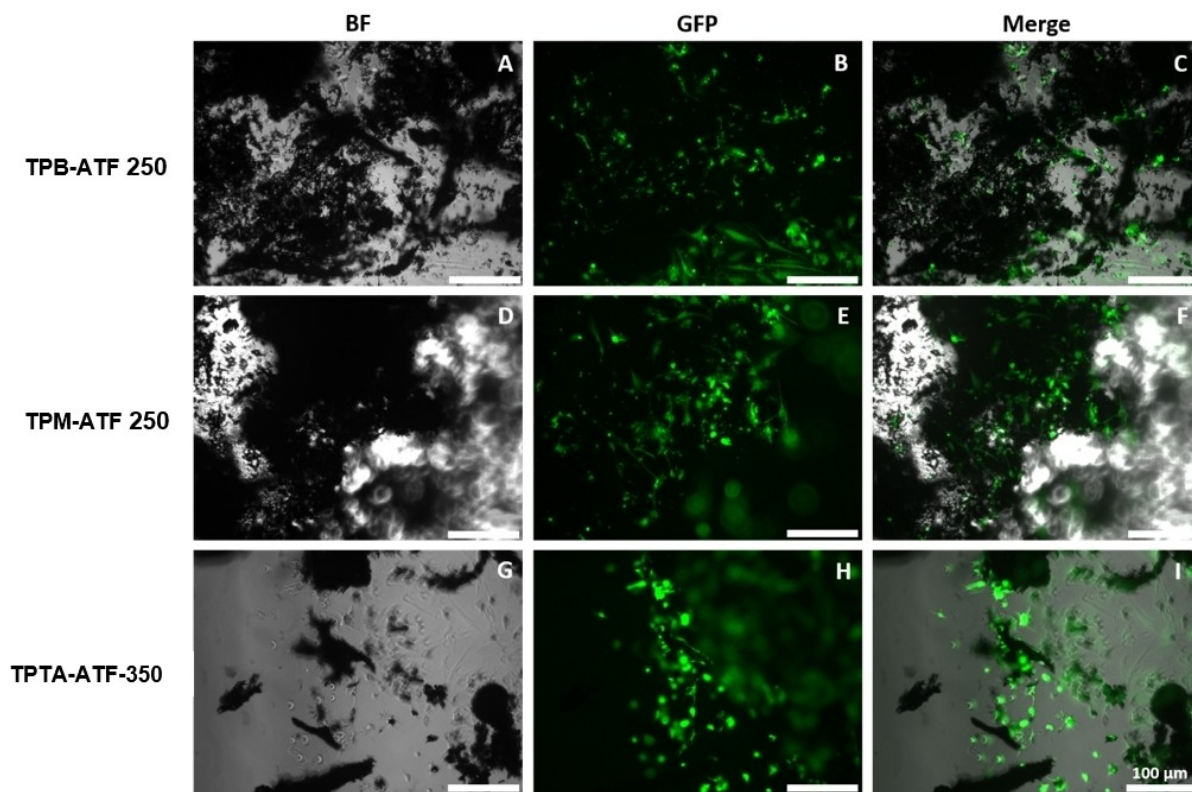


Figure 5. GFP expressing HUVEC grown on ATF networks after 24 h of incubation. A to C show the cells seeded on TPB-ATF 250, D to F the HUVEC on TPM-ATF 250, and G to I on cells on TPTA-ATF-350. A, D, and G are brightfield images of the probes, B, E, and H display the GFP fluorescent images (excitation 482 nm), and C, F, I show the merge of the brightfield and fluorescent images. Scale 100 μm , Leica DMI8 LED.

column structure (Figure 4A), which could also result from cut-off breaking. However, the image in Figure 4B, taken at higher magnification, shows intact columns and no damage. Large cavities with sizes up to several micrometers are visible in the framework (Figure 4B), indicating that nanometer-sized pores are accessible within the macroscopic structures. High-magnification SEM (Figure 4C) of a cone surface shows details with pores sizes between 10 nm and several 100 nm and cracks with a width of about 10 nm. We note that the surface is covered by a Pt layer with 12 nm thickness covering structural features with sizes distinctly below the Pt-layer thickness. This means that very small pores with sizes in the few-nanometer range may be present but cannot be detected in the SEM images.

Despite the trigonal planar core structure of the TPTA-ATF, no columnar structure can be observed by low-magnification SEM (supporting information, Figure S28), even though a marginally preferential growth is seen. Large cavities with sizes of several 10 μm occur. Also, growth with a preferred direction is not found for the ATF generated from the TPM core (supporting information, Figure S30) and TPE core (supporting information, Figure S32). The TPE-ATF structure is characterized by particularly large cavities with sizes up to 200 μm . High-magnification SEM shows similar pore sizes between 10 nm and several 100 nm and cracks with widths of about 10 nm for all three structures (Figure S29 for TPTA-ATF, Figure S31 for TPM-ATF, and Figure S33 for TPE-ATF). Again, smaller pores cannot

be detected because all structures are covered by a 12 nm Pt layer. Large coherent chunks can be found for Pc-ATF-250 in the overview. Strong π -stacking is assumed to be the reason why this framework cannot be expanded.

In summary, it can be found that there is a clear correlation between the macroscopic appearance of all ATFs and the corresponding SEM images. Depending on the geometry of the precursor, ATFs can be generated, which grow preferentially in one direction (TPB and TPTA) or without a defined direction of expansion (TPM and TPE). Trigonal core structures like azides **3** and **5** mainly expand perpendicular to their π -stacking plane, whereas the tetrahedral core TPM without a π -stacking plane expands in all directions. In the case of the TPE core, both expansion patterns were observed macroscopically depending on the crystallinity of the precursor.

2.2.6. ATF as biomaterials – cell adhesion assay

To investigate the adhesive properties of the ATFs, GFP expressing HUVEC (*human umbilical vein endothelial cells*) were seeded on top of the networks. Therefore the ATFs were attached to the bottom of an 8-well ibidi® slide using a thin layer of GelN/GelS hydrogel, which is reported to be non-toxic.^[11] Following 24 h of incubation, cell attachment was analyzed through fluorescence microscopy.

To visualize cell attachment to the ATFs, brightfield, and fluorescent images were merged, verifying the binding of HUVEC-GFP (Figure 5). Thus, proving adhesive properties for all tested ATF networks (TPB-ATF-250, TPM-ATF-250, TPTA-ATF-350). Furthermore, GFP production of HUVEC validates the viability of the cells. GFP-HUVECs nicely attach to the scaffolds and even migrate into the pores.

3. Conclusion

In conclusion, we reported the successful synthesis of seven azides with different core structures that can be synthesized from readily available aromatic building blocks. We then thermolyzed them to generate self-inflating porous organic frameworks called ATFs. Different building blocks lead to the formation of frameworks with different microscopic and macroscopic appearances depending on the respective core structure geometry. The appearance of the frameworks thermolyzed at 250 °C was examined by SEM. It was shown that the macroscopic appearance of the ATFs is reflected at the microscopic scale. IR spectroscopy revealed that the connection between the building blocks occurs by decomposition of the azide, generating a highly reactive nitrene which subsequently undergoes a C–H insertion, leading to the formation of secondary amines. Furthermore, we demonstrated that only aromatic azides could generate ATFs, whereas aliphatic azides decompose completely, and consequently, no framework formation can be observed.

Additionally, the elemental analysis gave insights into the elemental composition of the ATFs, showing that the formation of the framework is accompanied by a drastic loss of nitrogen, indicating that all azide functionalities decompose completely. Furthermore, the thermogravimetric analysis revealed that during thermolysis, the mass loss is constant in the range of temperatures between 250 °C and 450 °C. Therefore, the specific surface area for 250 °C, 350 °C, and 450 °C of the respective ATFs was determined according to the BET theory. It was shown that the SSA of the generated ATFs depends strongly on the temperature, revealing that higher temperatures result in an increased SSA and thus offer the possibility to control the specific surface area *via* the thermolysis temperature.

Furthermore, we investigated the adhesive properties of the ATFs by seeding GFP expressing HUVEC (*human umbilical vein endothelial cells*) on top of the network. We also investigate polyazides for the spin coating to prepare thin films. Besides this, we foresee many possible applications for these materials, like using sandwich structures for the adsorption of gases, biomaterials, membranes, or organic electronics. Furthermore, the possibility to incorporate metals in the phthalocyanine structure makes the Pc-ATF interesting for (metal) catalysis or conductivity.

Supporting Information

Supporting Information is available from the Wiley Online Library or the author. Additional references are cited within the Supporting Information.^[12–18]

Acknowledgements

This research has been funded by the Deutsche Forschungsgemeinschaft (DFG, German Research Foundation) under Germany's Excellence Strategy *via* the Excellence Cluster "3D Matter Made to Order" (3DMM2O, EXC-2082/1-390761711, Thrust A1 and A3).

We thank Dr. Stephan Grage for the solid-state NMR measurement and Micromeritics for the helium pycnometry. Open Access funding enabled and organized by Projekt DEAL.

Conflict of Interests

The authors declare no conflict of interest.

Data Availability Statement

The data that support the findings of this study are available from the corresponding author upon reasonable request.

Keywords: self-inflating · porous organic frameworks · multifunctional azides · nitrene precursors · adsorption

- [1] a) R. L. Siegelman, E. J. Kim, J. R. Long, *Nat. Mater.* **2021**, *20*, 1060; b) M. A. Little, A. I. Cooper, *Adv. Funct. Mater.* **2020**, *30*, 1909842; c) S. Das, P. Heasman, T. Ben, S. Qiu, *Chem. Rev.* **2017**, *117*, 1515; d) Y.-Z. Cheng, X. Ding, B.-H. Han, *ChemPhotoChem* **2021**, *5*, 406.
- [2] M. G. Mohamed, A. F. M. El-Mahdy, M. G. Kotp, S.-W. Kuo, *Materials Advances* **2022**, *3*, 707.
- [3] a) J.-X. Jiang, F. Su, A. Trewin, C. D. Wood, N. L. Campbell, H. Niu, C. Dickinson, A. Y. Ganin, M. J. Rosseinsky, Y. Z. Khimyak, A. I. Cooper, *Angew. Chem. Int. Ed.* **2007**, *46*, 8574; b) J. R. Holst, E. Stöckel, D. J. Adams, A. I. Cooper, *Macromolecules* **2010**, *43*, 8531.
- [4] W. Chaikittisilp, M. Kubo, T. Moteki, A. Sugawara-Narutaki, A. Shimojima, T. Okubo, *J. Am. Chem. Soc.* **2011**, *133*, 13832.
- [5] a) P. Pandey, O. K. Farha, A. M. Spokoyny, C. A. Mirkin, M. G. Kanatzidis, J. T. Hupp, S. T. Nguyen, *J. Mater. Chem.* **2011**, *21*, 1700; b) O. Plietzsch, C. I. Schilling, T. Grab, S. L. Grage, A. S. Ulrich, A. Comotti, P. Sozzani, T. Müller, S. Bräse, *New J. Chem.* **2011**, *35*, 1577.
- [6] A. P. Côté, A. I. Benin, N. W. Ockwig, M. O'Keeffe, A. J. Matzger, O. M. Yaghi, *Science* **2005**, *310*, 1166.
- [7] a) J. Mieres-Pérez, E. Mendez-Vega, K. Velappan, W. Sander, *J. Org. Chem.* **2015**, *80*, 11926; b) S. Bräse, C. Gil, K. Knepper, V. Zimmermann, *Angew. Chem. Int. Ed.* **2005**, *44*, 5188.
- [8] a) D. Göbel, N. Clamor, E. Lork, B. J. Nachtsheim, *Org. Lett.* **2019**, *21*, 5373; b) H. Takeuchi, K. Koyama, *J. Chem. Soc. Perkin Trans. 1* **1982**, DOI: 10.1039/p198200012691269.
- [9] S. Suárez-Pantiga, R. Hernández-Ruiz, C. Virumbrales, M. R. Pedrosa, R. Sanz, *Angew. Chem. Int. Ed.* **2019**, *58*, 2129.
- [10] S. Zhang, Q. Yang, C. Wang, X. Luo, J. Kim, Z. Wang, Y. Yamauchi, *Adv. Sci.* **2018**, *5*, 1801116.
- [11] T. Göckler, S. Haase, X. Kempter, R. Pfister, B. R. Maciel, A. Grimm, T. Molitor, N. Willenbacher, U. Schepers, *Adv. Healthcare Mater.* **2021**, *10*, 2100206.

- [12] S. Bräse, C. Gil, K. Knepper, V. Zimmermann, *Angew. Chem. Int. Ed.* **2005**, *44*, 5188.
- [13] a) D. Kvaskoff, H. Lüerssen, P. Bednarek, C. Wentrup, *J. Am. Chem. Soc.* **2014**, *136*, 15203; b) C. Wentrup, *Tetrahedron* **1974**, *30*, 1301; c) C. Wentrup, *Chem. Rev.* **2017**, *117*, 4562.
- [14] F. De Simone, T. Saget, F. Benfatti, S. Almeida, J. Waser, *Chemistry* **2011**, *17*, 14527.
- [15] X. Q. Guo, L. P. Zhou, L. X. Cai, Q. F. Sun, *Chemistry* **2018**, *24*, 6936.
- [16] S. A. Ceballos, S. Gil, A. M. Costero, *RSC Adv.* **2017**, *7*, 14279.
- [17] O. Plietzsch, C. I. Schilling, M. Tolev, M. Nieger, C. Richert, T. Müller, S. Bräse, *Org. Biomol. Chem.* **2009**, *7*, 4734.
- [18] M. Albakour, M. Zeyrek Ongun, S. Z. Topal, A. G. Gürek, *New J. Chem.* **2020**, *44*, 6285.

Manuscript received: May 8, 2023
 Revised manuscript received: May 29, 2023
 Accepted manuscript online: May 31, 2023
 Version of record online: ■ ■, ■ ■

RESEARCH ARTICLE

A selection of aromatic azides is synthesized and thermolyzed to obtain self-inflating Azide Thermolyzed Frameworks (ATFs). ATFs with preferential 2D or 3D growth directions are obtained depending on the building blocks' geometry. The molecular composition and properties of the ATFs are determined by BET, thermogravimetric analysis, IR, elemental analysis, and single electron microscopy.



*J. Brückel, Dr. Y. Matt, L. Schmidt, C. M. Mattern, U. Schepers, S. Leopold, M. Calkovsky, Prof. D. Gerthsen, Prof. S. Bräse**

1 – 11

**Azide Thermolysis Frameworks:
Self-inflating, Porous, and Light-
weight Materials**

